

# Direct and sequential contributions to the $^{26}\text{Mg}(^6\bar{\text{Li}},^6\text{He})^{26}\text{Al}$ reaction at 60 MeV

R. P. Ward \* and N. M. Clarke\*

*Wheatstone Laboratory, King's College London, Strand, London WC2R 2LS, England  
and School of Physics and Space Research, University of Birmingham, Edgbaston, Birmingham B15 2TT, England*

C. N. Pinder† and K. I. Pearce‡

*Wheatstone Laboratory, King's College London, Strand, London WC2R 2LS, England*

C. O. Blyth, H. D. Choi,<sup>§</sup> P. R. Dee, S. Roman, and G. Tungate

*School of Physics and Space Research, University of Birmingham, Edgbaston, Birmingham B15 2TT, England*

N. J. Davis

*Department of Physics, University of Edinburgh, Mayfield Road, Edinburgh EH9 3JZ, Scotland*

(Received 3 May 1993)

Angular distributions of differential cross-section and vector analyzing power have been measured for the  $^{26}\text{Mg}(^6\bar{\text{Li}},^6\text{He})^{26}\text{Al}$  reaction, populating four states in  $^{26}\text{Al}$ , at an incident energy of 60 MeV. Distorted-wave Born approximation (DWBA) calculations were performed for the  $(^6\bar{\text{Li}},^6\text{He})$  process using shell-model spectroscopic amplitudes and microscopic form factors derived from the M3Y interaction. Sequential contributions to the charge-exchange reaction mechanism via the  $(^6\bar{\text{Li}},^7\text{Li})(^7\text{Li},^6\text{He})$  and  $(^6\bar{\text{Li}},^7\text{Li}^*)(^7\text{Li}^*,^6\text{He})$  processes were calculated using the coupled-channels Born approximation (CCBA). The effects of inelastic couplings in  $^6\text{Li}$  were also examined.

PACS number(s): 24.70.+s, 25.70.Kk, 24.10.Eq, 27.30.+t

## I. INTRODUCTION

The small cross section of charge-exchange reactions and the weak beam currents associated with many polarized ion sources render polarization studies of such reactions difficult. Consequently, the only polarization studies of charge exchange which have been published are those where an intense beam is available, such as  $(n,p)$  and  $(p,n)$ , although studies of the  $^6\text{Li}(^3\text{He},t)^6\text{Be}$ ,  $^7\text{Li}(^3\text{He},t)^7\text{Be}$ , and  $^{48}\text{Ca}(^3\text{He},t)^{48}\text{Sc}$  reactions were performed using polarized  $^3\text{He}$  [1,2]. However, the only other study of polarized heavy-ion-induced charge exchange is that of Reber *et al.* [3], who investigated the  $^9\text{Be}(^6\bar{\text{Li}},^6\text{He})^9\text{B}$  reaction.

A larger body of work exists for charge-exchange reactions initiated by unpolarized beams. In particular, the  $^{26}\text{Mg}(^6\text{Li},^6\text{He})^{26}\text{Al}$  reaction was previously studied at bombarding energies between 32 and 210 MeV [4–6]. In their analysis of this reaction, Ciangaru *et al.* [5]

used a microscopic distorted-wave Born approximation (DWBA) approach and concluded that the conventional values of the nucleon-nucleon interaction strength could account for only 70% of the observed differential cross sections populating low-lying states in  $^{26}\text{Al}$ . This suggests that sequential processes might be of importance in the  $^{26}\text{Mg}(^6\bar{\text{Li}},^6\text{He})^{26}\text{Al}$  reaction.

The exact determination of direct and sequential contributions in charge exchange is difficult. There are uncertainties associated with the  $T = 1$  part of the nucleon-nucleon interaction even when the M3Y interaction is employed. The exact wave functions and spectroscopic amplitudes may also be unknown. For the sequential contributions, there remains the problem associated with the truncation of the model space when limiting the number of coupled channels. However, the calculation of sequential contributions to the  $(^6\bar{\text{Li}},^6\text{He})$  reaction is simplified by the fact that the stripping-pickup process  $(^6\bar{\text{Li}},^5\text{He})(^5\text{He},^6\text{He})$  is expected to be weak, as  $^5\text{He}$  is unbound and decays by neutron emission with a mean lifetime of order  $10^{-21}$  s. Thus, only pickup-stripping processes are expected to be important. This is in contrast to, for instance, the  $(t,^3\text{He})$  reaction, where the  $(t,\alpha)(\alpha,^3\text{He})$  and  $(t,d)(d,^3\text{He})$  processes are, in general, of equal importance [7,8]. A complication exists for the  $(^6\bar{\text{Li}},^6\text{He})$  reaction though, in that  $^7\text{Li}$  has a low-lying first-excited state ( $\frac{1}{2}^-$ , 0.478 MeV). Thus, one must calculate the contribution via the first-excited state of  $^7\text{Li}$ , that is,  $(^6\bar{\text{Li}},^7\text{Li}^*)(^7\text{Li}^*,^6\text{He})$ , in addition to that via the ground state of  $^7\text{Li}$ , that is,  $(^6\bar{\text{Li}},^7\text{Li})(^7\text{Li},^6\text{He})$ .

For the  $^{26}\text{Mg}(^6\bar{\text{Li}},^6\text{He})^{26}\text{Al}$  reaction, good shell-model calculations are available for the spectroscopic ampli-

\*Present address: School of Physics and Space Research, University of Birmingham, Edgbaston, Birmingham B15 2TT, England.

†Present address: Particle Physics Department, Rutherford Appleton Laboratory, Chilton, Didcot, Oxfordshire OX11 0QX, England.

‡Present address: Nuclear Electric, Berkeley Technology Centre, Berkeley, Gloucestershire GL13 9PB, England.

§Present address: Department of Physics, Kyungpook National University, Taegu 702-701, Korea (South).

tudes, but differential cross-section data is unable to distinguish accurately between the direct and sequential processes. However, calculations show that there are distinct differences between the vector analyzing powers (and to a lesser extent between the tensor analyzing powers) predicted by the direct and sequential contributions, so that it may be possible to separate the relevant contributions to the reaction from the analyzing powers. This formed the motivation for the present work.

## II. EXPERIMENT

The experiment was performed at the Nuclear Structure Facility, SERC Daresbury Laboratory. The  ${}^6\text{Li}$  beam, prepared by a polarized heavy ion source [9], was accelerated to 60 MeV by the tandem Van de Graaff accelerator [10]. The source was operated in two-phase mode, one phase having pure vector polarization and the other phase being unpolarized. Equal charges were incident on the target during each polarization phase; each polarization phase lasted typically 3 s. The data-acquisition system was inhibited during the period of the changeover between phases. In spectra, channels 2049–4096 corresponded to the polarized phase, while channels 4097–6144 corresponded to the unpolarized phase. In other polarization experiments using the same data-acquisition system, misrouting of data was found to be a problem. Thus, channels 1–2048 and 6145–8192 were not used in normal operation, but were allocated to misrouted data. However, no misrouting was observed during this experiment.

The experiment took place in the 700 mm diameter Charissa scattering chamber, using a self-supporting  ${}^{26}\text{Mg}$  target of  $500\ \mu\text{g cm}^{-2}$  nominal thickness. Ejectiles from scattering and reactions were detected by an array of eight silicon surface-barrier detector telescopes positioned symmetrically about the incident beam. Each telescope was equipped with a rectangular collimator and was located 300 mm from the target. The two most forward telescopes were equipped with collimators measuring 2 mm (in the reaction plane) by 5 mm (perpendicular to the reaction plane), while the remaining telescopes were equipped with collimators measuring 2 mm by 8 mm. Energy spectra were obtained for  ${}^6\text{Li}$ ,  ${}^7\text{Li}$ ,  ${}^6\text{He}$ ,  ${}^4\text{He}$ , and  ${}^8\text{Li}$  ejectiles, using the analog particle identifiers described by England [11]. A sample  ${}^6\text{He}$  spectrum is shown in Fig. 1, demonstrating that the energy resolution obtained for  ${}^6\text{He}$  ejectiles was approximately 150 keV. Differential cross-section and vector analyzing power data were obtained for the  $5^+$  ground,  $0^+$  (0.228 MeV),  $3^+$  (0.417 MeV), and  $1^+$  (1.058 MeV) states in  ${}^{26}\text{Al}$ . The  $0^+$  state, which is populated only via sequential nucleon transfers, was very weakly excited, in agreement with earlier studies [4,5]. The spin structure of the reaction populating the  $0^+$  state requires that  $iT_{11} = 0$  for all  $\theta$  [12]. At each angle,  $iT_{11}$  was calculated for this state and found to be statistically consistent with zero in all cases.

The polarization of the incident beam was monitored in a downstream polarimeter based around the polarimeter

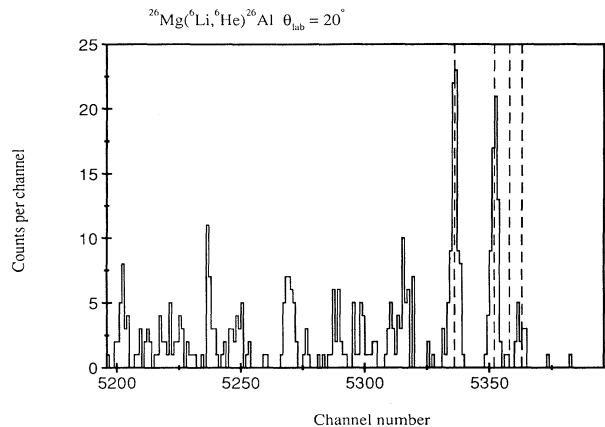


FIG. 1. Sample  ${}^6\text{He}$  spectrum from the  ${}^{26}\text{Mg}({}^6\text{Li}, {}^6\text{He}){}^{26}\text{Al}$  reaction at 60 MeV incident energy. The dashed lines indicate, from right to left, states in  ${}^{26}\text{Al}$  at excitation energies of 0, 0.228, 0.417, and 1.058 MeV, respectively.

assembly described by Karban *et al.* [9]. A deuterated polythene target of  $7\ \text{mg cm}^{-2}$  nominal thickness was used in this assembly. Two silicon detector telescopes were positioned at angles of  $\pm 23.5^\circ$  in the laboratory frame. As the beam was purely vector polarized, the  $0^\circ$  detector was omitted from this assembly. The beam was then stopped in an air-cooled Faraday cup located approximately 1 m downstream of the scattering chamber. An asymmetry of approximately  $\pm 0.15$  was observed for the  ${}^2\text{H}({}^6\text{Li}, {}^3\text{He}){}^5\text{He}$  reaction in these telescopes during the experiment. This asymmetry was used to monitor the polarization of the beam relative to an initial value of  $\tau_{10} = -0.65 \pm 0.04$  obtained prior to the start of the experiment. A beam-foil spectroscopy measurement [13] prior to the start of the experiment determined that the beam leaving the polarized ion source had a polarization consistent with the theoretical maximum of  $\tau_{10} = -0.82$  [14]. Depolarization during transport from the ion source to the scattering chamber was assumed to be  $(20 \pm 5)\%$ , based on the findings of Karban *et al.* [15] in their study of the scattering of polarized  ${}^7\text{Li}$ , yielding the initial value of  $\tau_{10} = -0.65 \pm 0.04$ . During the experiment, the polarization of the beam was found to vary between  $-0.66 \pm 0.04$  and  $-0.58 \pm 0.04$ . The beam current during the experiment averaged 20 nA (electrical).

Darden [16] demonstrated that the observed differential cross section  $\sigma(\theta)$  in a reaction initiated by a purely vector polarized beam of spin-1 particles is related to the unpolarized differential cross section  $\sigma_0(\theta)$  by

$$\sigma(\theta) = \sigma_0(\theta) \left( 1 + \sqrt{2}\tau_{10}iT_{11}(\theta) \sin\beta \cos\phi \right), \quad (1)$$

where  $iT_{11}(\theta)$  is the vector analyzing power of the reaction. The quantities  $\beta$  and  $\phi$  are angles describing the position of the spin-symmetry axis of the incident beam, and  $\tau_{10}$  is the vector polarization of the beam. In this experiment, it was arranged that  $\beta = 90^\circ$  and  $\phi = 0$ . Further details of the experiment have been given by Ward [17]. This paper reports the analysis of data

for the  $^{26}\text{Mg}(^6\bar{\text{Li}}, ^6\text{He})^{26}\text{Al}$  reaction. The analysis of the ( $^6\bar{\text{Li}}, ^6\text{Li}$ ) and ( $^6\bar{\text{Li}}, ^7\text{Li}$ ) data forms the basis of another paper [18].

### III. ANALYSIS

#### A. The Optical potential

The interaction between the projectile and target nuclei was described by the optical potential  $U(r)$  given by

$$U(r) = V_C(r) - V_0 f(x_0) - i \left( W_s f(x_s) - 4a_d W_d \frac{d}{dr} f(x_d) \right), \quad (2)$$

where the potential form factors  $f(x_n)$  have the Woods-Saxon shape given by

$$f(x_n) = (e^{x_n} + 1)^{-1} \quad (3)$$

and

$$x_n = \frac{r - r_n A^{1/3}}{a_n}, \quad (4)$$

where  $r_n$  and  $a_n$  are the reduced radius and diffuseness of the potential, respectively.  $V_C$  is the Coulomb potential due to a sphere of 1.25 fm reduced radius, and  $A$  is the mass number of the target nucleus.

The starting point of the analysis was a search to the differential cross-section data for elastic scattering using the optical-model search code HI-OPTIM [19]. The parameters derived from this search are shown as set 1 in Table I. The data could not be described acceptably using a Woods-Saxon derivative form for the imaginary potential. Parameters describing the interaction of  $^7\text{Li}$  with  $^{25}\text{Mg}$  were taken from the study by Cook *et al.* at 89 MeV [20]. These parameters are shown as set 2 in Table I. Parameters describing the interaction of  $^6\text{He}$  with  $^{26}\text{Al}$  were assumed to be set 1 in Table I also.

#### B. Shell-model calculations

The Michigan State University version [21] of the shell-model code OXBASH [22] was used to calculate one-body transition densities and spectroscopic amplitudes for the direct reaction mechanism. The formalism behind such calculations was described by Pinder *et al.* [8]. The results of these calculations are shown in Tables II and III.

TABLE I. Parameters for the CCBA analysis of data for the  $^{26}\text{Mg}(^6\text{Li}, ^6\text{He})^{26}\text{Al}$  reaction. Potential depths are in MeV and geometric parameters are in fm.

Set	$V_0$	$r_0$	$a_0$	$W_s$	$r_s$	$a_s$	$r_c$	Reference
1	166.430	1.150	0.847	15.663	2.010	0.727	1.250	[17]
2	142.740	1.300	0.800	36.880	1.300	0.800	1.250	[20]

TABLE II. Shell-model one-body transition densities (OBTD's) and spectroscopic amplitudes for transitions between the ground state of  $^{26}\text{Mg}$  and states in  $^{26}\text{Al}$ .

Transition	Create	Destroy	OBTD	Amplitude $\sqrt{S}$
$0_{\text{g.s.}}^+ \rightarrow 5_{\text{g.s.}}^+$	$1d_{5/2}$	$1d_{5/2}$	-0.46300	-0.4836
$0_{\text{g.s.}}^+ \rightarrow 3^+$	$1d_{3/2}$	$1d_{3/2}$	-0.00182	-0.0020
$0_{\text{g.s.}}^+ \rightarrow 3^+$	$1d_{3/2}$	$1d_{5/2}$	-0.06517	+0.0255
$0_{\text{g.s.}}^+ \rightarrow 3^+$	$1d_{5/2}$	$1d_{3/2}$	+0.02384	-0.0853
$0_{\text{g.s.}}^+ \rightarrow 3^+$	$1d_{5/2}$	$1d_{5/2}$	-0.05563	-0.0737
$0_{\text{g.s.}}^+ \rightarrow 3^+$	$1d_{5/2}$	$2s_{1/2}$	-0.14037	-0.4754
$0_{\text{g.s.}}^+ \rightarrow 3^+$	$2s_{1/2}$	$1d_{5/2}$	-0.36310	-0.1061
$0_{\text{g.s.}}^+ \rightarrow 1^+$	$1d_{3/2}$	$1d_{3/2}$	+0.02960	+0.0483
$0_{\text{g.s.}}^+ \rightarrow 1^+$	$1d_{3/2}$	$1d_{5/2}$	-0.01606	-0.1300
$0_{\text{g.s.}}^+ \rightarrow 1^+$	$1d_{3/2}$	$2s_{1/2}$	+0.03821	-0.0730
$0_{\text{g.s.}}^+ \rightarrow 1^+$	$1d_{5/2}$	$1d_{3/2}$	-0.07966	-0.0321
$0_{\text{g.s.}}^+ \rightarrow 1^+$	$1d_{5/2}$	$1d_{5/2}$	-0.44361	-0.8872
$0_{\text{g.s.}}^+ \rightarrow 1^+$	$2s_{1/2}$	$1d_{3/2}$	-0.04472	+0.0441
$0_{\text{g.s.}}^+ \rightarrow 1^+$	$2s_{1/2}$	$2s_{1/2}$	-0.10020	-0.1157

OXBASH was also used to calculate spectroscopic amplitudes for the sequential reaction mechanism calculations, with the results shown in Tables IV and V. Spectroscopic amplitudes for  $^6\text{Li} \rightarrow ^7\text{Li}_{\text{g.s.}}$ ,  $^6\text{Li} \rightarrow ^7\text{Li}^*$ , and  $^7\text{Li}_{\text{g.s.}} \rightarrow ^6\text{He}$  were calculated from the work of Cohen and Kurath [23]. The spectroscopic amplitude for the transition  $^7\text{Li}^* \rightarrow ^6\text{He}$  was calculated using OXBASH and was found to be equal to +0.862.

#### C. Direct charge-exchange form factors

Form factors for the direct charge-exchange reaction mechanism were calculated using the code CHEX2 [24], in conjunction with the one-body transition densities and spectroscopic amplitudes shown in Tables II and III. Both central and tensor parts of the M3Y ( $T = 1$ ) interaction were included in the calculation of the form factors, using the formalism described by Clarke and Cook [25].

#### D. Charge exchange

Charge-exchange calculations were performed using the King's College London version [26] of the coupled-channels code CHUCK [27,28]. Contributions from the ( $^6\text{Li}, ^7\text{Li}$ )( $^7\text{Li}, ^6\text{He}$ ) and ( $^6\text{Li}, ^7\text{Li}^*$ )( $^7\text{Li}^*, ^6\text{He}$ ) mechanisms

TABLE III. Shell-model spectroscopic amplitudes for transitions between the ground state of  $^6\text{Li}$  and the ground state of  $^6\text{He}$ .

Transition	Create	Destroy	Amplitude $\sqrt{S}$
$1_{\text{g.s.}}^+ \rightarrow 0_{\text{g.s.}}^+$	$1p_{1/2}$	$1p_{1/2}$	+0.101
$1_{\text{g.s.}}^+ \rightarrow 0_{\text{g.s.}}^+$	$1p_{3/2}$	$1p_{1/2}$	-0.965
$1_{\text{g.s.}}^+ \rightarrow 0_{\text{g.s.}}^+$	$1p_{1/2}$	$1p_{3/2}$	+0.648
$1_{\text{g.s.}}^+ \rightarrow 0_{\text{g.s.}}^+$	$1p_{3/2}$	$1p_{3/2}$	+0.936

TABLE IV. Shell-model spectroscopic amplitudes for transitions between the ground state of  $^{26}\text{Mg}$  and states in  $^{25}\text{Mg}$ .

Transition	Transfer	Amplitude $\sqrt{S}$
$0_{\text{g.s.}}^+ \rightarrow 5_{2\text{g.s.}}^+$	$1d_{5/2}$	-1.58691
$0_{\text{g.s.}}^+ \rightarrow 1_{2}^+$	$2s_{1/2}$	-0.41493

were calculated using the coupled-channels Born approximation (CCBA) and the zero-angle finite-range approximation (ZAFRA) [29], while contributions from direct charge exchange were calculated using the zero-range DWBA. The coupling scheme used is shown in Fig. 2. For  $^6\text{Li}$ - and  $^7\text{Li}$ -induced charge exchange, the techniques used in this analysis are known to yield results essentially identical to those obtained by Williams-Norton *et al.* [30] for the  $^{40}\text{Ca}(^7\text{Li}, ^7\text{Be})^{40}\text{K}$  reaction and by Cook and Kemper [31] for the  $^9\text{Be}(^6\text{Li}, ^6\text{He})^9\text{B}$  reaction. The CHUCK calculations of Clarke and Cook [25] for the  $^{16}\text{O}(^7\text{Li}, ^7\text{Be})^{16}\text{N}$  reaction have also been checked using the finite-range code FRESKO [32]; the CHUCK and FRESKO calculations were found to agree within (10–15)%. CHUCK calculations for other reactions have also been checked against finite-range DWBA and no-recoil DWBA calculations [29].

### 1. $5^+$ state of $^{26}\text{Al}$

The direct reaction mechanism populating the  $5^+$  ground state of  $^{26}\text{Al}$  produces the steeply decreasing differential cross section shown as a dotted line in Fig. 3. The sequential reaction mechanisms  $(^6\text{Li}, ^7\text{Li})(^7\text{Li}, ^6\text{He})$

TABLE V. Shell-model spectroscopic amplitudes for transitions between states in  $^{25}\text{Mg}$  and states in  $^{26}\text{Al}$ .

Transition	Transfer	Amplitude $\sqrt{S}$
$5_{2\text{g.s.}}^+ \rightarrow 5_{\text{g.s.}}^+$	$1d_{5/2}$	-1.02469
$5_{2\text{g.s.}}^+ \rightarrow 0^+$	$1d_{5/2}$	-1.58691
$5_{2\text{g.s.}}^+ \rightarrow 3^+$	$1d_{5/2}$	-0.21374
$5_{4\text{g.s.}}^+ \rightarrow 3^+$	$1d_{3/2}$	+0.14602
$5_{5\text{g.s.}}^+ \rightarrow 3^+$	$2s_{1/2}$	-0.80295
$5_{2\text{g.s.}}^+ \rightarrow 1^+$	$1d_{5/2}$	-1.18160
$5_{4\text{g.s.}}^+ \rightarrow 1^+$	$1d_{3/2}$	+0.12320
$1_{2}^+ \rightarrow 5_{\text{g.s.}}^+$		
$1_{2}^+ \rightarrow 0^+$	$2s_{1/2}$	-0.41493
$1_{2}^+ \rightarrow 3^+$	$1d_{5/2}$	-0.44474
$1_{2}^+ \rightarrow 1^+$	$1d_{3/2}$	-0.16264
$1_{2}^+ \rightarrow 1^+$	$2s_{1/2}$	-0.20067

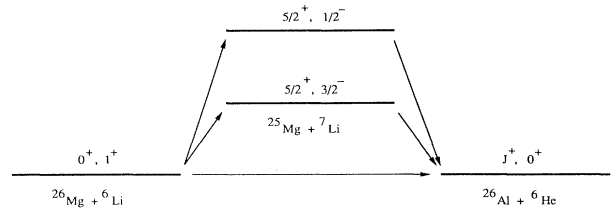


FIG. 2. Coupling scheme for charge-exchange calculations. The first spin parity refers to the target/residual nucleus, while the second refers to the projectile/ejectile nucleus.

and  $(^6\text{Li}, ^7\text{Li}^*)(^7\text{Li}^*, ^6\text{He})$  produce contributions depicted as dashed and dot-dashed lines respectively. The phase of the cross-section data resembles that of the  $(^6\text{Li}, ^7\text{Li})(^7\text{Li}, ^6\text{He})$  contribution rather than those of the other two mechanisms. However, no single mechanism reproduces the data.

The resultant of the three mechanisms is shown as a

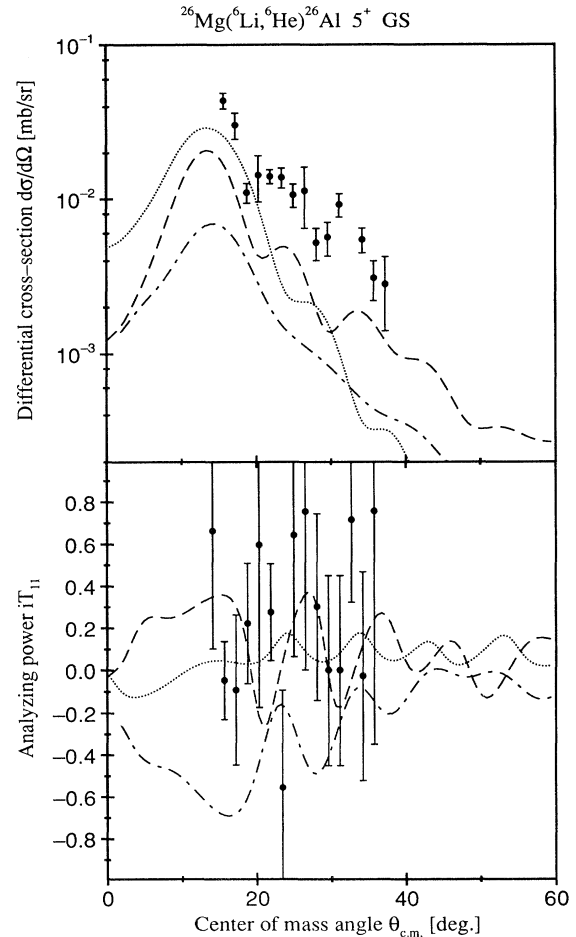


FIG. 3. CCBA predictions for the  $^{26}\text{Mg}(^6\text{Li}, ^6\text{He})^{26}\text{Al}$  reaction populating the  $5^+$  ground state of  $^{26}\text{Al}$ . The direct,  $(^6\text{Li}, ^7\text{Li})(^7\text{Li}, ^6\text{He})$ , and  $(^6\text{Li}, ^7\text{Li}^*)(^7\text{Li}^*, ^6\text{He})$  reaction mechanisms are the dotted, dashed, and dot-dashed lines, respectively.

dashed line in Fig. 4. Neither the magnitude nor the phase of the differential cross-section data is reproduced. In attempt to improve the description of the data, the signs of the amplitudes for the  ${}^7\text{Li} \rightarrow {}^6\text{He}$  and  ${}^7\text{Li}^* \rightarrow {}^6\text{He}$  transitions were reversed. This modification yielded the solid line in Fig. 4, which reproduces the differential cross-section data very well.

The analyzing power data for this state are statistically poor. However, calculations including the direct and sequential mechanisms are consistent with the data.

## 2. $0^+$ state of ${}^{26}\text{Al}$

This state in  ${}^{26}\text{Al}$  is populated only by sequential nucleon transfers. The mechanisms  $({}^6\text{Li}, {}^7\text{Li})({}^7\text{Li}, {}^6\text{He})$  and  $({}^6\text{Li}, {}^7\text{Li}^*)({}^7\text{Li}^*, {}^6\text{He})$  populating this state are shown as the dashed and dot-dashed lines in Fig. 5. The resultant of the two mechanisms is shown as a solid line; all calculations predict  $iT_{11} = 0$  for all  $\theta$ . Clearly, the  $({}^6\text{Li}, {}^7\text{Li}^*)({}^7\text{Li}^*, {}^6\text{He})$  process is very important in the pop-

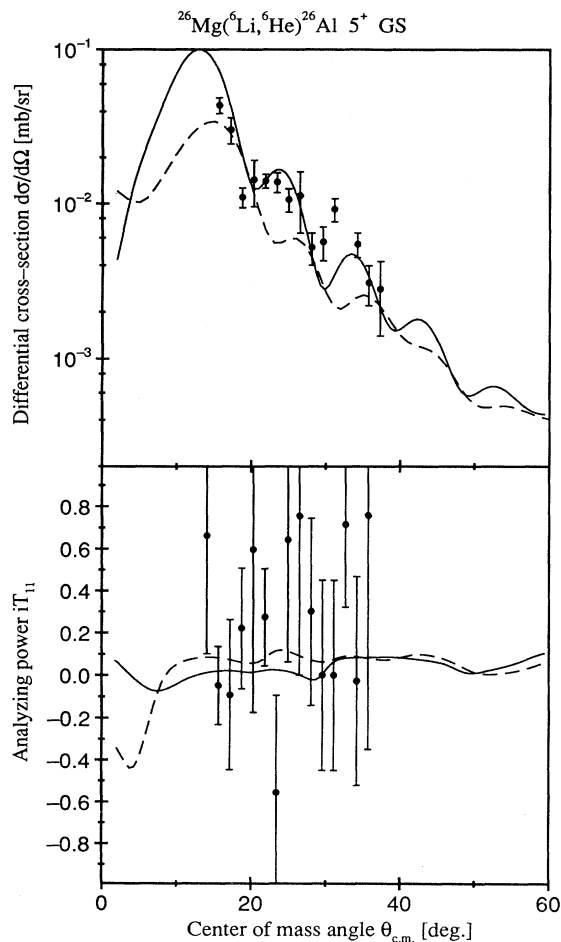


FIG. 4. CCBA predictions for the  ${}^{26}\text{Mg}({}^6\text{Li}, {}^6\text{He}){}^{26}\text{Al}$  reaction populating the  $5^+$  ground state of  ${}^{26}\text{Al}$ . The dashed line is the resultant of the direct and sequential mechanisms, while the solid line is the resultant with the signs of the amplitudes for the  ${}^7\text{Li} \rightarrow {}^6\text{He}$  and  ${}^7\text{Li}^* \rightarrow {}^6\text{He}$  transitions reversed.

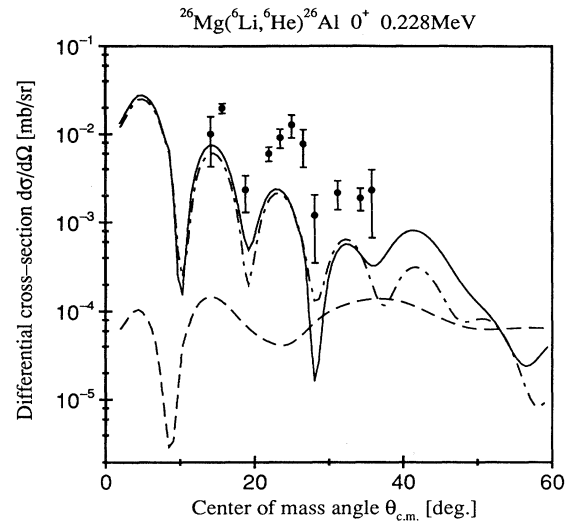


FIG. 5. CCBA predictions for the  ${}^{26}\text{Mg}({}^6\text{Li}, {}^6\text{He}){}^{26}\text{Al}$  reaction populating the  $0^+$  state of  ${}^{26}\text{Al}$ . The  $({}^6\text{Li}, {}^7\text{Li})({}^7\text{Li}, {}^6\text{He})$  and  $({}^6\text{Li}, {}^7\text{Li}^*)({}^7\text{Li}^*, {}^6\text{He})$  reaction mechanisms are the dashed and dot-dashed lines, respectively. The solid line is the resultant of the two sequential mechanisms.

ulation of this state. The phase of the data is reproduced, although the magnitude is underpredicted by a factor of approximately 2. Similar results were obtained by Duhm *et al.* [4] in their analysis of data for this state at a bombarding energy of 32 MeV. It is inferred from this that the sequential predictions presented in this paper for other states in  ${}^{26}\text{Al}$  are also accurate to within a factor of 2.

## 3. $3^+$ state of ${}^{26}\text{Al}$

The direct reaction mechanism populating this state is shown as a dotted line in Fig. 6. Neither the magnitude nor the phase of the data is reproduced. The phase, although not the magnitude, of the data is correctly reproduced by the  $({}^6\text{Li}, {}^7\text{Li})({}^7\text{Li}, {}^6\text{He})$  reaction mechanism, shown as a dashed line in Fig. 6. The  $({}^6\text{Li}, {}^7\text{Li}^*)({}^7\text{Li}^*, {}^6\text{He})$  contribution is an order of magnitude smaller than that due to the other two mechanisms. The resultant of the direct and sequential mechanisms is shown as a solid line in Fig. 6. This calculation reproduces the phase of the differential cross-section data, although the magnitude is slightly underpredicted.

The analyzing power generated by the direct reaction mechanism has a phase similar to the data but is small in magnitude and mostly positive, whereas the data show large negative values. In contrast, the analyzing powers generated by the two sequential mechanisms are similar to the data in both phase and magnitude. The resultant of the direct and sequential mechanisms reproduces the analyzing power data very well.

## 4. $1^+$ state of ${}^{26}\text{Al}$

The direct reaction mechanism predicts the observables shown as the dotted lines in Fig. 7. The magnitude

of the differential cross-section data is quite well reproduced, although a slight phase difference exists between prediction and data. The  $({}^6\text{Li}, {}^7\text{Li})({}^7\text{Li}, {}^6\text{He})$  mechanism is shown as a dashed line in Fig. 7 and reproduces the position of the first and third maxima of the data rather well. The  $({}^6\text{Li}, {}^7\text{Li}^*)({}^7\text{Li}^*, {}^6\text{He})$  mechanism is shown as a dot-dashed line in Fig. 7; this contribution has a phase similar to that of the other sequential contribution, although a slightly smaller magnitude. However, no mechanism alone reproduces the phase and magnitude of the cross-section data. The predictions for  $iT_{11}$  are interesting in that, while the direct mechanism predicts small, positive analyzing powers, both sequential mechanisms predict highly oscillatory analyzing powers.

The resultant of the direct and sequential mechanisms is shown as a dashed line in Fig. 8. For the differential cross section, the addition of the sequential reaction mechanisms has damped the oscillations resulting from the direct reaction. However, the structure of the ana-

lyzing power data is not reproduced.

In an effort to improve the description of the analyzing power data for this state, the signs of the amplitudes for the  ${}^7\text{Li} \rightarrow {}^6\text{He}$  and  ${}^7\text{Li}^* \rightarrow {}^6\text{He}$  transitions were reversed. This procedure yielded the predictions depicted as solid lines in Fig. 8. The resultant of the two mechanisms reproduces the analyzing power data quite well. While the direct reaction mechanism generates large cross sections and weak analyzing powers, the sequential mechanisms produce smaller cross sections and large analyzing powers. It is thus the analyzing power data which is most sensitive to sequential processes.

### E. Projectile excitation effects

Vector analyzing powers for the elastic scattering of  ${}^6\text{Li}$  by  ${}^{26}\text{Mg}$  are known to be generated by inelastic excitations in  ${}^6\text{Li}$  [17,18,33,34]. Coupling between the ground

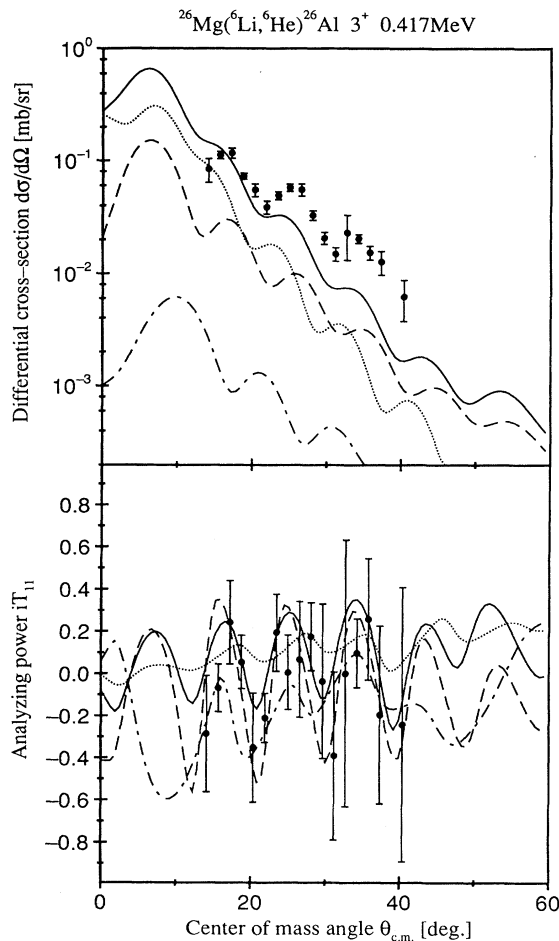


FIG. 6. CCBA predictions for the  ${}^{26}\text{Mg}({}^6\text{Li}, {}^6\text{He}){}^{26}\text{Al}$  reaction populating the  $3^+$  state of  ${}^{26}\text{Al}$ . The direct,  $({}^6\text{Li}, {}^7\text{Li})({}^7\text{Li}, {}^6\text{He})$ , and  $({}^6\text{Li}, {}^7\text{Li}^*)({}^7\text{Li}^*, {}^6\text{He})$  reaction mechanisms are the dotted, dashed, and dot-dashed lines, respectively. The solid line is the resultant of the direct and sequential mechanisms.

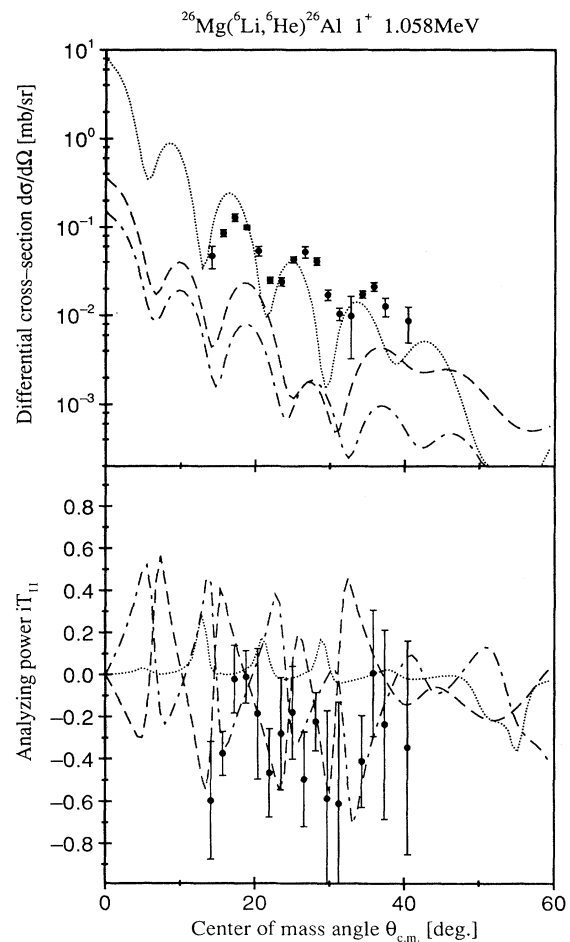


FIG. 7. CCBA predictions for the  ${}^{26}\text{Mg}({}^6\text{Li}, {}^6\text{He}){}^{26}\text{Al}$  reaction populating the  $1^+$  state of  ${}^{26}\text{Al}$ . The direct,  $({}^6\text{Li}, {}^7\text{Li})({}^7\text{Li}, {}^6\text{He})$  and  $({}^6\text{Li}, {}^7\text{Li}^*)({}^7\text{Li}^*, {}^6\text{He})$  reaction mechanisms are the dotted, dashed, and dot-dashed lines, respectively.

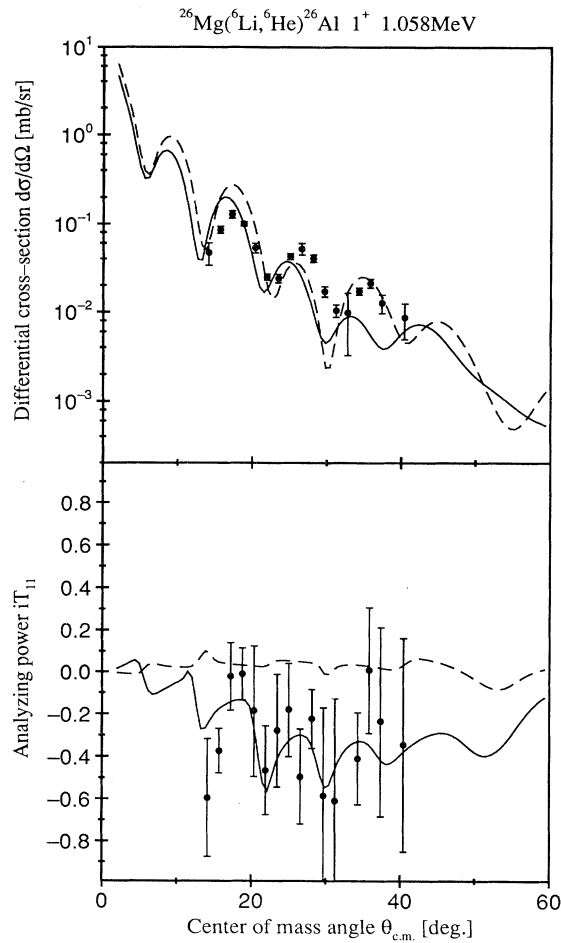


FIG. 8. CCBA predictions for the  $^{26}\text{Mg}(^6\text{Li}, ^6\text{He})^{26}\text{Al}$  reaction populating the  $1^+$  state of  $^{26}\text{Al}$ . The dashed line is the resultant of the direct and sequential mechanisms, while the solid line is the resultant with the signs of the amplitudes for the  $^7\text{Li} \rightarrow ^6\text{He}$  and  $^7\text{Li}^* \rightarrow ^6\text{He}$  transitions reversed.

TABLE VI. Scaling factors  $f$  for  $^6\text{Li}$  excitation calculations.  $S$  is the spin of the projectile,  $J$  is the spin of the target,  $S'$  is the spin of the ejectile, and  $J'$  is the spin of the residual nucleus. The quantities  $l$ ,  $s$ , and  $j$  are the angular momentum associated with the coupling, the angular momentum transfer in the projectile, and the angular momentum transfer in the target, respectively.

$S$	$J$	$S'$	$J'$	$l$	$s$	$j$	$f$
1	0	1	0	2	2	0	1.581
1	0	3	0	2	2	0	2.070
3	0	3	0	2	2	0	-1.936
1	0	2	0	2	2	0	2.738
2	0	2	0	2	2	0	-1.337
1	0	1	0	2	2	0	1.581
1	0	1	0	2	2	0	1.581

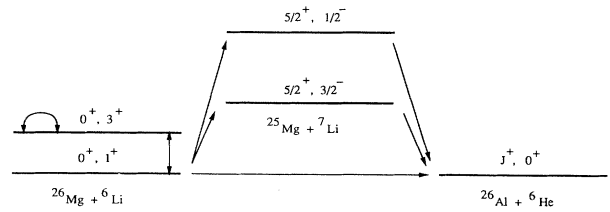


FIG. 9. Coupling scheme for charge-exchange calculations including inelastic excitation of the projectile. The first spin parity refers to the target/residual nucleus, while the second refers to the projectile/ejectile nucleus.

state of  $^6\text{Li}$  and the  $3^+$  excited state at 2.18 MeV generates an analyzing power having the correct phase but too large a magnitude. Couplings between the ground state of  $^6\text{Li}$  and the  $2^+$  and  $1^+$  excited states at 4.31 MeV and 5.65 MeV then reduce the magnitude of the vector analyzing power.

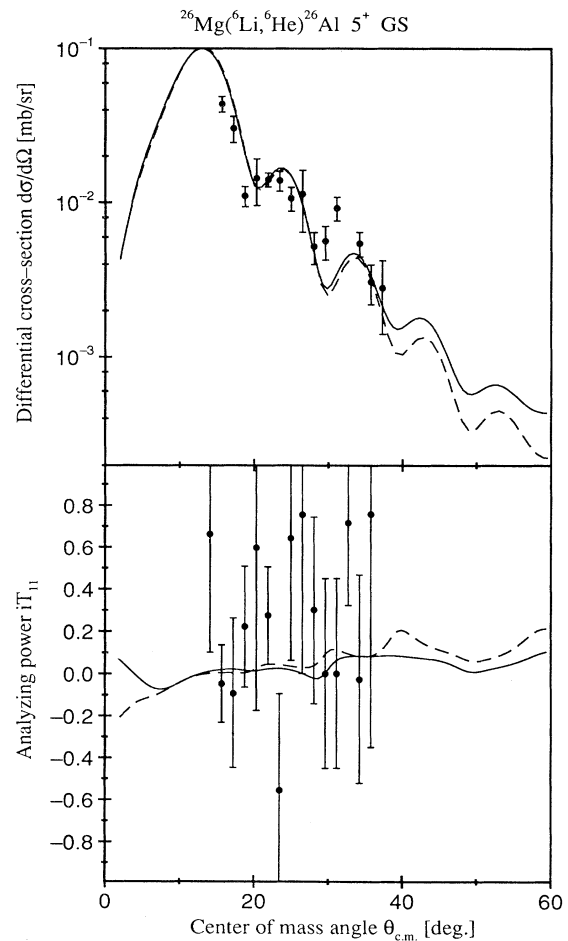


FIG. 10. CCBA predictions for the  $^{26}\text{Mg}(^6\text{Li}, ^6\text{He})^{26}\text{Al}$  reaction populating the  $5^+$  state of  $^{26}\text{Al}$ . The dashed line is the result of calculations including couplings in  $^6\text{Li}$ , while the solid line is the full CCBA calculation without the couplings in  $^6\text{Li}$ .

A detailed description of the application of CHUCK to projectile excitation calculations for  ${}^7\text{Li}$  scattering was given by Cook *et al.* [35]. They demonstrated that it was necessary to scale the coupling strengths by a factor dependent on the spins and isospins of the coupled states. The corresponding factors for  ${}^6\text{Li}$  excitation calculations are tabulated in Table VI.

The charge-exchange calculations were extended to include coupling between the  $1^+$  ground and  $3^+$  excited states of  ${}^6\text{Li}$ , using the coupling scheme depicted in Fig. 9. Figure 10 shows the full calculation extended to include coupling between the ground and  $3^+$  states of  ${}^6\text{Li}$  and reorientation of the  $3^+$ . The value of the coupling strength for the  $1^+ \leftrightarrow 3^+$  transition in  ${}^6\text{Li}$  was chosen to correspond to a deformation length  $\delta_2 = 2.19$  fm, this value being intermediate between the values 2.34 fm and 1.89 fm derived from measurements of the differential cross section for  ${}^6\text{Li}$  inelastic excitation [36]. The  $3^+ \leftrightarrow 3^+$  reorientation coupling in  ${}^6\text{Li}$  was included with a coupling strength corresponding to  $\delta_2 = -1.10$  fm, this value being  $-0.5$  times the coupling strength for the  $1^+ \leftrightarrow 3^+$  transition [37]. Figure 10 demonstrates that even with this coupling strength, the predicted observables were modified only slightly. Clearly, projectile excitation effects are of secondary importance, the structure of the observables being largely determined by the reaction mechanism.

#### IV. CONCLUSIONS

CCBA calculations have been performed for the  ${}^{26}\text{Mg}({}^6\bar{\text{Li}}, {}^6\text{He}){}^{26}\text{Al}$  reaction populating four states in  ${}^{26}\text{Al}$ . Calculations of the direct reaction mechanism, with form factors based on the shell model, underestimated the observed differential cross sections for

the  $5^+$  and  $3^+$  states. For the  $5^+$  ground state of  ${}^{26}\text{Al}$ , this anomaly was removed when the sequential reaction mechanisms  ${}^{26}\text{Mg}({}^6\bar{\text{Li}}, {}^7\text{Li})({}^7\text{Li}, {}^6\text{He}){}^{26}\text{Al}$  and  ${}^{26}\text{Mg}({}^6\bar{\text{Li}}, {}^7\text{Li}^*)({}^7\text{Li}^*, {}^6\text{He}){}^{26}\text{Al}$  were included. For the  $3^+$  excited state of  ${}^{26}\text{Al}$  at  $E_x = 0.417$  MeV, the data were still underpredicted when the sequential reaction mechanism had been included, although the phase of the data was accurately reproduced. For the  $1^+$  state of  ${}^{26}\text{Al}$  at  $E_x = 1.058$  MeV, the structure and magnitude of the data were well reproduced, but a slight phase difference remained between prediction and data even when the sequential contributions were included. Differential cross-section data for the  $0^+$  state of  ${}^{26}\text{Al}$ , which is populated only by sequential nucleon transfers and is thus a stringent test of the accuracy of sequential reaction mechanism calculations, were reproduced within a factor of 2. It is inferred that the sequential calculations for the other states are also accurate to within a factor of 2.

For the  $5^+$ ,  $3^+$ , and  $1^+$  states, the direct reaction mechanism generated small vector analyzing powers, whereas the sequential mechanisms generated larger, more oscillatory analyzing powers. Vector analyzing power data for the  $3^+$  and  $1^+$  states were reproduced only when direct and sequential reaction mechanisms were included. The predictions for these states indicate that, at this energy, the structure of the analyzing powers is generated by interference between the direct and sequential contributions. Inelastic excitation of the  ${}^6\text{Li}$  projectile was also included in the calculations and was found to have only a small effect on the predictions.

This work was supported in part by the Science and Engineering Research Council of the United Kingdom under Grants No. GR/F/39874 (to King's College London) and No. GR/H/23825 (to the University of Birmingham).

- 
- [1] A.K. Basak, O. Karban, S. Roman, G.C. Morrison, C.O. Blyth, and J.M. Nelson, *Nucl. Phys.* **A368**, 74 (1981).
  - [2] N.M. Clarke, *J. Phys. G* **10**, 917 (1984).
  - [3] E.L. Reber, K.W. Kemper, P.L. Kerr, A.J. Mendez, E.G. Myers, B.G. Schmidt, and N.M. Clarke, *Phys. Rev. C* **47**, 2190 (1993).
  - [4] H.H. Duhm, H. Hafner, R. Renfordt, M. Goldschmidt, O. Dragun, and K.-I. Kubo, *Phys. Lett.* **48B**, 1 (1974).
  - [5] G. Ciangaru, R.L. McGrath, and F.E. Cecil, *Nucl. Phys.* **A380**, 147 (1982).
  - [6] J.S. Winfield, N. Anantaraman, Sam M. Austin, Ziping Chen, A. Galonsky, J. van der Plicht, H.-L. Wu, C.C. Chang, and G. Ciangaru, *Phys. Rev. C* **35**, 1734 (1987).
  - [7] K.I. Pearce, N.M. Clarke, R.J. Griffiths, P.J. Simmonds, A.C. Dodd, D. Barker, J.B.A. England, M.C. Mannion, and C.A. Ogilvie, *Phys. Rev. C* **35**, 1617 (1987).
  - [8] C.N. Pinder, C.O. Blyth, N.M. Clarke, D. Barker, J.B.A. England, B.R. Fulton, O. Karban, M.C. Mannion, J.M. Nelson, C.A. Ogilvie, L. Zybert, R. Zybert, K.I. Pearce, P.J. Simmonds, and D.L. Watson, *Nucl. Phys.* **A533**, 25 (1991).
  - [9] O. Karban, W.C. Hardy, K.A. Connell, S.E. Darden, C.O. Blyth, H.D. Choi, S.J. Hall, S. Roman, and G. Tungate, *Nucl. Instrum. Methods A* **274**, 4 (1989).
  - [10] J.S. Lilley, *Phys. Scr.* **25**, 435 (1982).
  - [11] J.B.A. England, *Nucl. Instrum. Methods* **106**, 45 (1973).
  - [12] P. Zupranski, W. Dreves, P. Egelhof, E. Steffens, D. Fick, and F. Rösel, *Nucl. Instrum. Methods* **167**, 193 (1979).
  - [13] H. Jänsch, E. Koch, W. Dreves, and D. Fick, *J. Phys. D* **17**, 231 (1984).
  - [14] D.B. Steski (private communication).
  - [15] O. Karban, G. Kuburas, C.O. Blyth, H.D. Choi, S.J. Hall, S. Roman, G. Tungate, Z. Moroz, I.M. Turkiewicz, G. Grawert, and N.J. Davis, *Nucl. Phys.* **A528**, 465 (1991).
  - [16] S.E. Darden, in *Proceedings of the Third International Symposium on Polarization Phenomena in Nuclear Reactions*, Madison, 1970, edited by H.H. Barschall and W. Haeberli (University of Wisconsin Press, Madison, 1971), p. 39.
  - [17] R.P. Ward, Ph.D. thesis, University of London, 1992.
  - [18] R.P. Ward, N.M. Clarke, K.I. Pearce, C.N. Pinder,

- C.O. Blyth, H.D. Choi, P.R. Dee, S. Roman, G. Tun-  
gate, and N.J. Davis (unpublished).
- [19] N.M. Clarke, optical-model computer code HI-OPTIM,  
University of Birmingham, UK, 1991.
- [20] J. Cook, N.M. Clarke, and R.J. Griffiths, *Nucl. Phys.*  
**A357**, 246 (1981).
- [21] B.A. Brown, W.E. Ormand, and J.S. Winfield, Michi-  
gan State University version of the shell-model computer  
code OXBASH, Michigan State University Report No. 524,  
1986.
- [22] A. Etchegoyen, W.D.M. Rae, N.S. Godwin, W.A. Richter  
and C.H. Zimmerman, shell-model computer code  
OXBASH, University of Oxford, 1982.
- [23] S. Cohen and D. Kurath, *Nucl. Phys.* **A101**, 1 (1967).
- [24] N.M. Clarke, direct charge-exchange form-factor com-  
puter code CHEX2, University of Birmingham, UK, 1985.
- [25] N.M. Clarke and J. Cook, *Nucl. Phys.* **A458**, 137 (1986).
- [26] N.M. Clarke, King's College London version of the  
coupled-channels computer code CHUCK, 1990.
- [27] P.D. Kunz, coupled-channels computer code CHUCK, Uni-  
versity of Colorado, 1978.
- [28] J.R. Comfort, extended version of the coupled-channels  
computer code CHUCK, Arizona State University, 1979.
- [29] N.M. Clarke, *J. Phys. G* **10**, 1219 (1984).
- [30] M.E. Williams-Norton, F. Petrovich, K.W. Kemper,  
R.J. Puigh, D. Stanley, and A.F. Zeller, *Nucl. Phys.*  
**A313**, 477 (1979).
- [31] J. Cook and K.W. Kemper, *Phys. Rev. C* **31**, 1745  
(1985).
- [32] I.J. Thompson, *Comput. Phys. Rep.* **7**, 167 (1988).
- [33] K. Rusek, J. Giroux, H.J. Jansch, H. Vogt, K. Becker,  
K. Blatt, A. Gerlach, W. Korsch, H. Leucker, K. Luck,  
H. Reich, H.-G. Volk, and D. Fick, *Nucl. Phys.* **A503**,  
223 (1989).
- [34] Y. Hirabayashi and Y. Sakuragi, *Nucl. Phys.* **A536**, 375  
(1992).
- [35] J. Cook, N.M. Clarke, J. Coopersmith, and R.J. Griffiths,  
*Nucl. Phys.* **A386**, 346 (1982).
- [36] S.P. Van Verst, D.P. Sanderson, D.E. Trcka, K.W. Kem-  
per, V. Hnizdo, B.G. Schmidt, and K.R. Chapman, *Phys.*  
*Rev. C* **39**, 853 (1989).
- [37] M.F. Vineyard, J. Cook, and K.W. Kemper, *Phys. Rev.*  
*C* **31**, 879 (1985).